Toxicology International, *31(1) : 19-32; 2024. DOI: 10.18311/ti/2024/v31i1/35255*

Online ISSN : 0976-5131; Print ISSN : 0971-6580

Toxicology International

Contents available at: www.informaticsjournals.com/index.php/toxi



Isotherm and Kinetic Studies on Adsorption of Yellow Azo Dyes (Sunset Yellow, Tartrazine) using *Kigelia africana* (Lam.) Benth., Leaf Extract Mediated Iron Nanoparticles

N. Usha Rani[1*], K. Ramanjaneyulu[2], P. Pavani[1] and S. L. Tulasi[1]

[1]Department of Freshman Engineering, P. V. P. Siddhartha Institute of Technology, Kanuru, Vijayawada - 520 007, Andhra Pradesh, India; nannapaneniusharani73@gmail.com

[2]Department of Electronics and Communication Engineering, PVP Siddhartha Institute of Technology, Vijayawada - 520 007, Andhra Pradesh, India

Abstract

Sunset yellow and tartrazine are commonly used azo dyes extensively employed in beverages and food products such as soda, fruit juices, confectionery, and cakes. These dyes hold the distinction of being the second and third most frequently utilized colour additives in a wide array of beverage products. The discharge of these synthetic food dyes into industrial wastewater can lead to significant environmental and health issues. Due to its aromatic structure, this dye is resistant to breaking down into harmless compounds, and its removal through effective adsorption presents an economical and efficient solution. The use of renewable bioresources for the eco-friendly production of metallic nanoparticles represents a recent and growing trend in nanotechnology research, offering enhanced environmental safety. In this current research, we achieved the green and cost-effective synthesis of monodispersed Iron Nanoparticles (FeNPs) with exceptional stability by utilizing an aqueous extract of *Kigelia africana* (Lam.) Benth is the primary bioresource for this synthesis. The FeNPs were noticed to be uniformly distributed spherical-shaped particles having smooth surfaces with a 26-34 nm size range and an average particle size of 28 ± 0.86 nm. The XRD results confirm that the FeNPs were rhombohedral phase structures with 71.43% of elemental iron. These synthesized nanoparticles were applied for the removal of sunset yellow and tartrazine dyes were investigated and more than 90% were removed. The adsorption isotherm study was best fitted with the Langmuir model, and the maximal adsorption capacity was found to be 76.29 and 47.22 mg/g for sunset yellow and tartrazine respectively. The adsorption reaction follows pseudo-first-order kinetics with a high correlation coefficient. Repeated cycles of regeneration, reuse and stability showed very high removal efficiency and stability. In conclusion, the biosynthesis of metal nanoparticles demonstrates substantial promise for applications in environmental protection.

Keywords: Adsorption Studies, Characterisation, *Diospyros chloroxylon*, Green Synthesis, Iron Nanoparticles, *Kigelia africana*, Sunset Yellow, Tartrazine

**Author for correspondence*

Article Received on: 02..10.2023 Revised on: 15.06.2023 Accepted on: 30.06.2023

1. Introduction

Water stands as a vital resource for sustaining life on our planet and fostering human progress. Among anthropogenic activities, the textile industry ranks as one of the most significant consumers and polluters of water bodies[1]. The textile industry has a global presence, generating approximately $1 trillion in revenue, accounting for 7% of the total worldwide exports, and providing employment to roughly 35 million workers across the globe[2].

The textile industry bears a significant burden of environmental consequences, with its primary impact stemming from the release of untreated effluents into water bodies, which typically account for 80% of its total emissions[3]. These effluents commonly contain elevated levels of biochemical oxygen demand and chemical oxygen demand due to the presence of substantial quantities of non-biodegradable organic compounds, notably textile dyes, found in the wastewater generated by this industry[4,5].

Sunset yellow and tartrazine are prevalent azo dyes commonly found in beverages and food products such as confectionery, fruit juices, soda and cakes. These dyes rank as the second and third most frequently utilized colour additives in various beverage items[6]. Notably, they display remarkable resistance to factors such as light, oxygen, and pH fluctuations, rendering them an appealing choice for manufacturers. Moreover, they offer a more cost-effective alternative to natural dyes. However, it's worth noting that sunset yellow and tartrazine have been linked to potential mutagenic and carcinogenic properties due to the presence of azo groups[7]. In response to these concerns, several northern European countries, including Finland and Norway, have already instituted bans on the use of sunset yellow as a precautionary measure[8].

Hence, it is imperative to implement treatment methodologies that prioritize environmental sustainability for future generations. These strategies can encompass a mixture of physical, chemical, and biological technologies[9]. It's worth noting that while physical-chemical methods have shown effectiveness, they come with challenges such as managing generated sludge and incurring high costs related to electricity, inputs, and operations. Furthermore, bioabsorption can come into play, particularly when the dye exhibits high toxicity to microorganism growth. This process involves the absorption, deposition, and ion exchange, employing nanoparticles, deceased bacteria, yeasts, and fungi[10].

More recently, green synthesized nanoparticles have gained prominence in water treatment due to their non-toxic, cost-effective, and environmentally friendly nature[11]. The high dye reduction efficiency of nanoparticles was due to their high specific surface area, small particle size, and reactivity[12]. Because of this, the study intended to synthesize FeNPs utilizing leaf extract of *Kigelia africana* (Lam.) Benth., as a reducing and capping agent. The characterization of synthesized nanoparticles was conducted with different characterization techniques. Further, the nanoparticles were applied as a catalyst for the removal of carcinogenic yellow azo dyes such as sunset yellow and tartrazine in an aqueous solution

2. Materials and Methods

2.1 Collection of Plant Material

Healthy leaves from the *Kigelia africana* plant were brought from Seshachalam Hills in Tirupati, Andhra Pradesh. The collected plant material was verified and authenticated by Dr. Ch. Srinivasa Reddy, Assistant Professor, Department of Botany, SRR and CVR Government Degree College (A) Vijayawada, whose voucher specimen number SRR-CVR/ 2023/PI/01 was deposited at Department of Botany. To ensure cleanliness, the gathered leaves underwent a thorough cleaning process, which included removing sand and dirt using sterile cotton and rinsing with distilled water. Subsequently, any remaining water droplets on the cleaned leaves were eliminated using tissue paper. The plant material was finely chopped into small pieces and delicately dried in the shade. The dried leaf material was stored in an amber-coloured glass bottle for future use.

2.2 Extract Preparation

Dried leaves of *Kigelia africana* were utilized to prepare an aqueous leaf extract. The leaves were powdered to a consistent size using a mortar and pestle, and precisely 20 grams of the leaf powder were boiled for 20 minutes in 250 mL of double-distilled water at 60°C. Subsequently, the extracts underwent filtration through nylon mesh and a hydrophilic 0.2 µ millipore filter to eliminate impurities and this extract was utilized for fabrication of FeNPs[13].

2.3 Synthesis of FeNPs

The *Kigelia africana* aqueous leaf extract-derived nanoparticles were synthesized by adopting the procedure reported previously[13,14]. Sample solutions were created

in a 1:10 ratio by adding 2 mL of the extract to 20 mL of 8, 10, 12 and 15 mM $Fe_2SO_4 \cdot 7H_2O$ solutions at room temperature, in 100 ml Erlenmeyer flasks. To prepare various concentrations of iron salt solutions, a stock solution was initially made in 50 mL of distilled water. The solutions were continuously stirred for 8 hours at 60-70 °C, followed by additional stirring at 37°C for 24 hours. The nanoparticles formed in the reaction mixture were collected by centrifugation followed by followed by washing with distilled water. Then the obtained nanoparticles were collected by drying in an air oven.

2.4 Characterization

The initial reaction's colour change, indicative of nanoparticle formation, was verified using UV-visible spectral analysis on a double-beam UV-visible spectrophotometer (JASCO, Japan) with a scan range of 800-300 nm. The formation of nanoparticles and the identification of phytochemical groups were assessed through FTIR analysis conducted on a Bruker (USA) instrument within the 500-4000 cm^{-1} range. The structural characterization of nanoparticles was carried out using Transmission Electron Microscopy (TEM) and Energy-Dispersive X-ray spectroscopy (EDX). The TEM analysis was conducted on a Jeol JEM 2100 instrument operating at 120 keV. Before analysis, the nanoparticles were carefully washed with methanol and then mounted on carbon-coated copper grids. Crystal size and elemental composition were evaluated using a Jeol 6390LA SEM instrument coupled with OXFORD XMX-N EDX, operated with a Tungsten lamp at an accelerating voltage of 0.5 to 30 kV. X-Ray Diffraction (XRD) analysis was performed on a Bruker D8 Advance EDX instrument, utilizing Cu Kα radiation, with the nanoparticles washed multiple times with ethanol to prevent sodium chloride crystallization. The scan range was set at 2θ of 20-100^0.

2.5 Adsorption Methodology

The dye adsorption experiment was performed as per the procedure reported in the literature[15]. To initiate the experiments, stock solutions of tartrazine and sunset yellow dyes were prepared at a concentration of 0.5 g/L separately in distilled water. Subsequently, these stock solutions were further diluted to the desired concentrations during the experimental study. The absorbance values of both dyes were determined using a UV spectrophotometer. The adsorption experiments were conducted at room temperature and were carried out using an automatic shaker to ensure consistent reactions. Various experimental parameters, including dosage, contact time, initial dye concentration, pH levels, the presence of interfering salts, and temperature variations were varied. In each experiment performed, the adsorption capacity equilibrium (q_e) and metal removal (R in %) were calculated for both nanoparticles using the formula

$$qe = \frac{Ci - Ce \times V}{m} \quad (1)$$

$$R(\%) = \frac{Ci - Ce \times V}{Ci} \quad (2)$$

where, Ci = metal ion initial concentration; Ce = metal ion equilibrium concentration; V = volume of metal solution in L and m = weight of nanoparticles taken as adsorbent.

2.6 Adsorption Kinetic Studies

The investigation of adsorption kinetics stands as a pivotal aspect in the rational design of industrial adsorption processes. The dye reduction efficiency kinetics of synthesised nanoparticles was conducted in a series of experiments conducted within 250 mL Erlenmeyer flasks. Each flask contained 0.2 grams (equivalent to 2 g/L) of nanoparticles, combined with a 100 mL dye suspension containing dyes at their respective required concentrations, all adjusted to their optimum pH and temperature conditions.

These suspensions were maintained at a constant temperature of 30 ± 0.2 °C while being agitated at 200 rpm using a shaker. Samples were collected at various time intervals until equilibrium was reached. Subsequently, these samples were subjected to analysis, and the percentage removal of dye or metals was determined utilizing Equation (2).

To gain insights into the dynamics of dye adsorption by synthesized nanoparticles, we conducted a kinetic study employing both the Lagergren pseudo-first-order and chemisorption's pseudo-second-order kinetics models. The Lagergren pseudo-first-order equation is as follows

$$(qe - qt) = lnqe - K1\ t \quad (3)$$

This equation served as a basis for the evaluation of the adsorption kinetics. In the equation qt (mg/g^{-1}) represents the adsorption capacity at a given time 't' and qe (mg/g) is

the adsorption capacity at equilibrium (mg/g), $K1$ (min^{-1}) stands for the pseudo-first-order rate constant.

The pseudo-second-order kinetic model can be expressed in its linear form as follows

$$t/q_t = 1/K_2q^2_e + t/q_t \quad (4)$$

where, K_2 represents the pseudo-second-order rate constant in g mg^{-1} min^{-1}.

2.7 Adsorption Isothermal Study

The equilibrium concentrations along with their corresponding adsorption efficiency were utilized to construct adsorption isotherms. These isotherms were generated in the concentration range of 5-100 mg/L for both dyes and experiments were conducted under their respective optimal pH and temperature conditions. All other parameters and sample analyses were carried out following the previously described methods. The equilibrium concentration of adsorbed metal (q_e) was determined using Equation (1).

The adsorption isotherm represents the relationship between the quantity of a substance adsorbed per unit mass of adsorbent at a constant temperature and its concentration in the equilibrium solution. The Langmuir and Freundlich isotherms are the two most commonly utilized models to depict data on adsorption from a solution.

2.7.1 Langmuir Isotherm

The Langmuir isotherm is relevant when the adsorption of the adsorbate is constrained to a single layer on the surface of the adsorbent. The linear representation of the Langmuir isotherm is expressed by the following equation:

$$Ce/qe = 1/ KL.Q0 + Ce/Q0 \quad (5)$$

The potential for the adsorption process can be assessed through the separation factor (R_L), which can be computed using the following equation:

$$RL = 1/1+KLC0 \quad (6)$$

where, KL represents the Langmuir constant and C_0= is the concentration of the dye solution prepared. R_L indicates the isotherm to be unfavourable (RL>1), linear (RL=1), irreversible (RL=0) or favourable (0<RL<1).

2.7.2 Freundlich Isotherm

The empirical Freundlich model, which describes adsorption on a heterogeneous surface, is expressed by the following equation:

$$qe = ln\, KF + \ln c_e \quad (7)$$

where, KF represents Freundlich constants related expressed in mg/g and n represents adsorption favourability.

2.8 Stability and Recyclability of Nanoparticles

The stability of synthesized nanoparticles was evaluated chemically by mixing 0.1 g of synthesized nanoparticles with 200 mL of aqueous solution at a wide pH range i.e., from 2.0 to 10. Then the reaction mixture was kept in an orbital shaker for 24 h at 75°C. The iron ions dissolved in the solution were evaluated using an atomic absorption spectrophotometer.

The recyclability of the synthesized nanoparticles plays a significant role as the particles were recyclable, it will reduce the experimental cost. The nanoparticles after completion of the metal reduction study were washed with 0.01 M hydrochloric acid, EDTA separately and then washed several times with distilled water. The particles were dried for 24 h at 60 °C and then were utilized for an adsorption study the same procedure was repeated 5 times and based on the results, the reusability was evaluated[16].

3. Results and Discussion

Kigelia Africana extract facilitated the successful synthesis of FeNPs through an environmentally friendly approach. The reaction mixture, composed of a 1:10 ratio of extract to $FeSO_4{\cdot}7H_2O$, underwent a noticeable colour transformation from yellow to black following overnight agitation at 37°C. This alteration in colour signified the role of phytoconstituents from *Kigelia africana* in effectively reducing Fe into nanoparticles. The initial reduction of metal ions initiated the formation of a nucleation centre, promoting the accumulation of additional metal ions and the integration of adjacent nucleation sites. The nanoparticles were formed as a result which becomes entrapped with biological molecules of the plant for better stability and improved morphology.

The UV scanning spectra of the synthesized FeNPs exhibited highly intense absorption maxima at 558 nm suggesting the formation of nanoparticles. Different strengths of salts utilized for the fabrication of nanoparticles produce the same wavelength maxima but different absorption intensities. The absorption intensity was increased with an increase in the metal ion strength

to 12 mM (Figure 1) and then decreased suggesting that the 12 mM concentration of metal ion was considered to be very favourable for the fabrication of nanoparticles. The UV absorption maxima noticed for the synthesized FeNPs were well correlated with the findings reported in literature[17-19]. These spectral changes strongly suggest the active involvement of biomolecules within the leaf extract of *Kigelia africana* in the process of nanoparticle formation.

The identification of functional groups involved in the synthesis of FeNPs from an aqueous extract of *Kigelia africana* was conducted through FTIR spectroscopy. In Figure 2, the absorbance bands of FeNPs are depicted within the wavenumber in the scanning range of 500 to 4000 cm^{-1}. Notable peaks were recognized at 3396 cm^{-1} and 1353 cm^{-1} corresponding to O-H stretching and O-H bending indicative of the presence of phenol or alcohol as a functional group. The band at 1547 cm^{-1} represents C=C bending in aromatic compounds. The presence of C=O stretching in aldehyde was confirmed by observing the band at 1735 cm^{-1}. Additionally, the band at 1644 cm-1 confirms C=C stretching, attributing it to the alkene functional group. Our findings align with previous studies, affirming the involvement of O–H and C=O bonds attributed to phenol/alcohol and alkene functional groups in both the synthesis and stability of FeNPs derived from *Kigelia africana*.

The microstructure and crystallinity of FeNPs synthesized in the study were examined through TEM. The high-resolution TEM image reveals that the FeNPs exhibit a spherical shape with an average diameter ranging from 26 to 34 nm. The particle size obtained from TEM closely corresponds to that derived from Dynamic Light Scattering (DLS). Further analysis indicates a spacing of approximately 0.22 nm between the planes, which is consistent with the planes of the biosynthesized silver

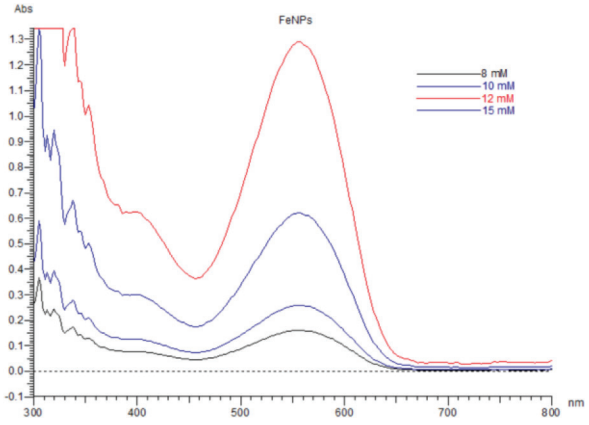


Figure 1. UV-visible absorption spectra of FeNPs.

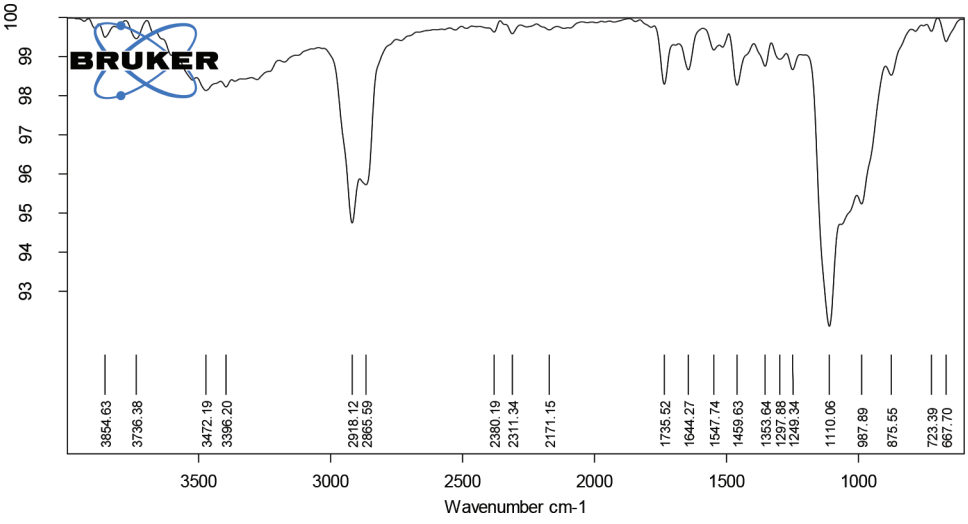


Figure 2. FTIR Spectrum for FeNPs.

nanoparticles. The crystalline nature of the particles is evident in the Selected Area Electron Diffraction (SAED) pattern, where bright spots are observed. Analysis of the image allowed the identification of diffraction planes corresponding to the crystalline FeNPs with a rhombohedral phase structure.

The hydrodynamic size of synthesised FeNPs was determined to be 28 ± 0.86 nm, with a Polydispersity Index (PDI) value of 0.38 ± 0.07. Additionally, the FeNPs exhibited an average zeta potential of -11 ± 0.7 mV. The zeta potential measurements provide insights into the stability of nanoparticle solutions, with particles tending to agglomerate as the electric potential approaches zero. Notably, particles are inclined to repel each other when the zeta potential is either more than +20 mV or less than -20 mV.

Furthermore, EDX analysis (Figure 4) was performed to assess the elemental composition of the nanoparticles. The EDX spectrum indicates that the particles comprise 71.43% elemental iron. The presence of carbon and oxygen in the spectrum is attributed to phytochemical constituents responsible for the reduction of elemental iron into FeNPs. Additionally, signals corresponding to chloride were observed, likely originating from the nanoparticle synthesis process. The various characterizations of the synthesized nanoparticles were found to be in good agreement with the existing literature[20-22].

The XRD analysis (Figure 5) provided confirmation related to crystal phases, crystallinity, and particle size of the FeNPs synthesized in the study. The XRD spectrum exhibited well-defined diffraction reflections at 2θ values at 24.25, 33.09, 35.63, 40.89, 49.51, 54.12, 57.63, 62.39, 64.03 and 72.36 corresponding to (012), (104), (110), (113), (024), (116), (018), (214), (300), and (119), indicating a rhombohedral phase structure for the particles. These Bragg reflections were consistent with the standard JCPDS card no 33-0664. The absence of other diffraction patterns related to impurities in the XRD results suggests that the obtained particles were highly pure. Applying the Debye-Scherrer equation for crystal size evaluation revealed a particle size of 28 nm, which aligns well with the sizes observed in SEM and TEM analyses. The XRD results are in correlation with the findings presented in literature[20-22].

3.1 Adsorption Study

The dye adsorption efficiency of the synthesized FeNPs was evaluated by optimizing various experimental conditions

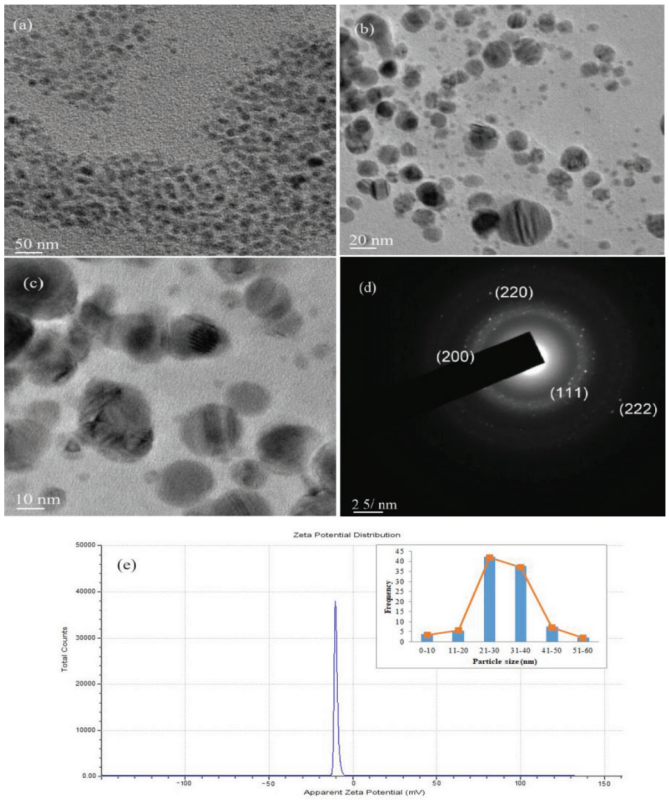


Figure 3. TEM, particle size distribution and zeta potential analysis results of synthesised FeNPs.

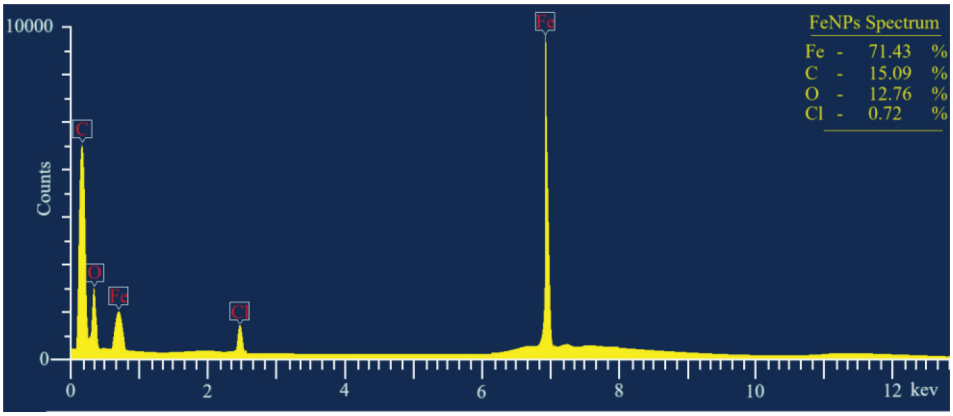


Figure 4. EDX spectrum of FeNPs.

such as concentration of dye, dose of adsorbent, time of adsorption, pH of solution and agitation rate. All the adsorption experiments were performed in triplicate and results were expressed as average

The efficiency of the photocatalyst in catalyzing reactions is significantly influenced by the pH of the reaction medium. In this study, the photocatalytic performance of synthesized FeNPs was assessed across 2-10 pH values for both sunset yellow and tartrazine. The pH adjustments were achieved using 0.1 M NaOH and 0.1 M H_2SO_4. The experiments were conducted with synthesized nanoparticles under visible light irradiation for 120 min, maintaining a 0.5 g/L adsorbent dosage and 100 µg/mL dye concentration. The observed photocatalytic efficiency of the synthesized FeNPs exhibited a direct correlation with the pH of the dye solution. As the pH of the solution increased from 2 to 10, there was a concurrent decrease in the degradation of both dyes studied. This phenomenon is attributed to the alteration of surface properties in response to varying pH levels for nanoparticles. As the dyes in the study were anionic and showed high adsorption efficiency with positively charged catalyst surfaces and hence increase in adsorption was noticed with a decrease in the pH of the reaction mixture. This enhancement in photocatalytic efficiency under visible light irradiation culminates in the degradation of MB dye, reaching up to 78.52 ± 0.137 % for sunset yellow and 81.53 ± 0.213 % for tartrazine (Figure 6(A)).

To assess the influence of dye concentration on the catalytic degradation efficiency, experiments were conducted at optimized pH and an irradiation time of 120 min, with the initial dye concentration ranging from 5 to 100 mg/L. Before UV-visible light irradiation, the dye solutions containing nanoparticles were allowed to reach adsorption–desorption equilibrium in the dark for 30 min. The percentage removal of dye solutions, spanning concentrations from 5 to 100 mg/L, was approximately 20%-25% after the 30 min adsorption in the dark. Photocatalytic degradation was then initiated under UV-visible light irradiation, with the assumption of time t = 0. The results clearly illustrate an inverse relationship between the degradation efficiency of the catalyst and the initial dye concentration of MB and Rh B. As the initial dye concentration increases, the time required for complete degradation elongates, leading to a decrease in photocatalytic proficiency. Higher concentrations of the dye result in a greater number of dye molecules being adsorbed on the catalyst surface, causing reduced light penetration. The optimum high % adsorption was noticed at a concentration of 25 mg/L and 50 mg/L with % adsorption of 87.79 ± 0.337 % for sunset yellow and 88.57 ± 0.209 % for tartrazine. The results of this study are summarized in Figure 6(B).

The reaction mixture agitation rate of 25 to 150 rpm was studied to evaluate the dye adsorption efficiency of synthesized nanoparticles. Based on results as shown in Figure 6(C), it was observed that the dye removal efficiency of both nanoparticles was very low at a low agitation rate and then went on to increase with the increase in the agitation rate up to 100 rpm for both dyes. An agitation rate of 125 and 150 rpm, the % adsorption was noticed to be decreased and hence 100 rpm was selected as the optimized agitation rate for the adsorption of dyes using synthesized FeNPs.

The impact of photocatalyst weight on dye degradation was investigated while maintaining constant experimental conditions. The percentage degradation of both dyes by the nanocatalyst was assessed at various catalyst doses ranging from 0.25 to 1.0 gm/L. It was observed that the initial degradation rate increased with higher catalyst concentrations, reaching a maximum, as illustrated in Figure 6(D). The augmentation in catalyst

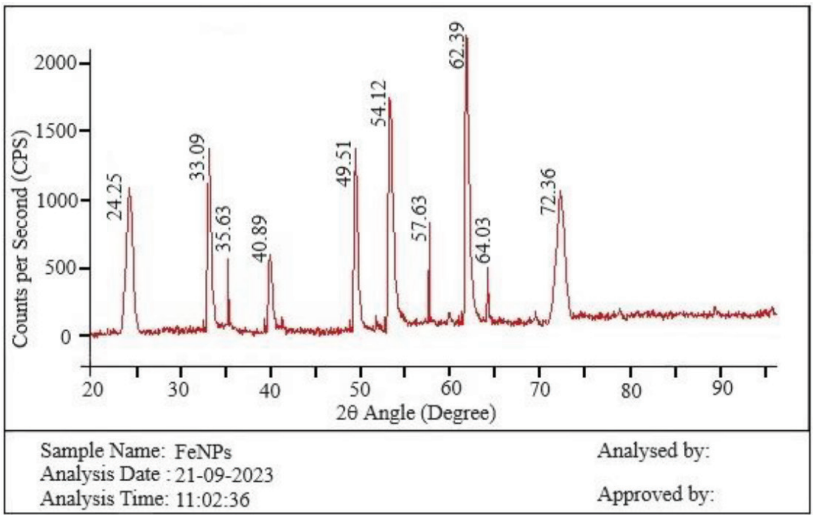


Figure 5. XRD analysis results of FeNPs.

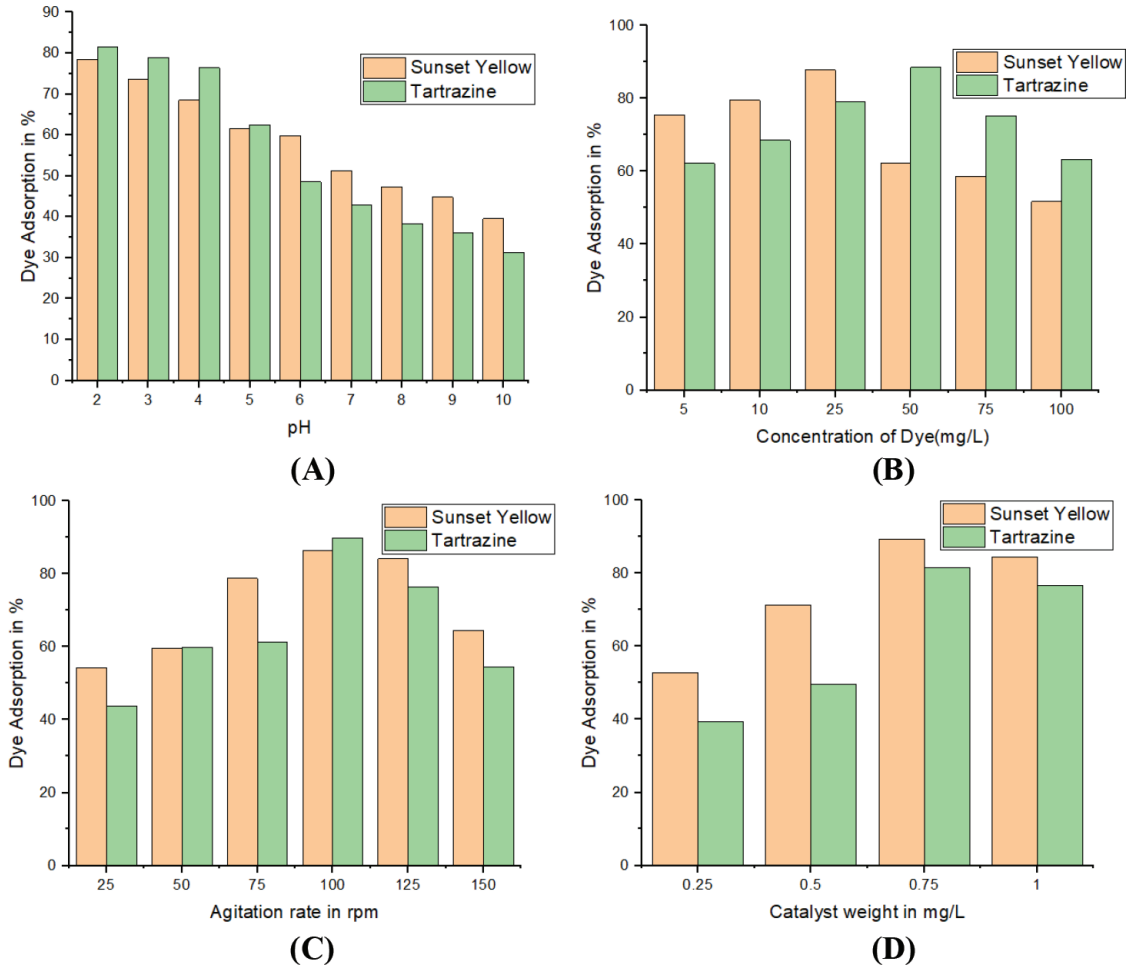


Figure 6. Optimization of experimental parameters. **(A)** pH of the reaction mixture. **(B)** dye concentration. **(C)** agitation rate. **(D)** nano adsorbent dose.

concentration led to an increased absorption of photons and a higher number of dye molecules being degraded, thereby enhancing the degradation rate. The maximum adsorption was noticed with an adsorbent dose of 0.75 g/L with an adsorption efficiency of 89.36% and 81.56% respectively for sunset yellow and tartrazine. The heightened percentage of adsorption with an increased adsorbent dose can be attributed to the expanded surface area of the adsorbent and the availability of more adsorption sites. However, the rate of adsorption began to decline as the adsorbent dose continued to increase beyond the optimal value. This decline is primarily due to the overlap of adsorption sites, resulting from an overabundance of adsorbent particles.

To determine the optimal adsorption time demonstrating maximum adsorption, a series of adsorption times ranging from 15 to 90 minutes were investigated. This assessment was conducted while keeping the reaction mixture's pH, agitation rate, dye strength, and the dose of the nano adsorbent at optimized levels. The UV-visible spectrophotometer was employed to quantify the amount of dye adsorbed. Figure 7 presents the UV-visible absorption spectra of both untreated and nanoparticle-treated dye solutions. The illustration depicts a notable decrease in dye concentration, indicating a reduction within the aqueous dye solution.

The contact time versus adsorption of sunset yellow and tartrazine using synthesised FeNPs was presented in Figure 8. The adsorption of sunset yellow and tartrazine was noticed at a % of 72.25 ± 0.099 and 69.36 ± 0.436 using synthesized FeNPs as adsorbent within a short period of 45 min. This evidence that, the process of dye adsorption is initiated with the rapid adsorption of dye onto the surface of nanoparticles. This initial phase of adsorption gradually decelerates once most of the available active sites become saturated. The adsorption at 75 min contact time was noticed to be 90.24 ± 0.326 and 94.58 ± 0.309 % for sunset yellow and tartrazine respectively. This study suggests that the nanoparticles possess high adsorption efficiency towards carcinogenic dyes in the study.

3.2 Adsorption Isotherm Model

The adsorption data of sunset yellow and tartrazine was subjected to fitting with two distinct isotherm models such as Langmuir and Freundlich. This was done to establish a correlation between our experimental findings and these models. The model that provided the best fit to the data exhibited an exceptional correlation coefficient (R^2) equal to unity. The Langmuir isotherm model posits that adsorption entails a monolayer formation process, wherein each active site accommodates one dye ion, and all these sites are energetically equivalent, with no interaction among adsorbed ions. Our results demonstrated that the experimental data for the adsorption of dye on synthesized FeNPs exhibited a strong fit with the Langmuir isotherm model.

The correlation coefficient noticed in Langmuir isothermal graph was noticed to be very close to 1 suggesting that the monolayer adsorption was favorable in the study. The q_{max} (mg/g) was noticed to be very high for the studied dyes suggesting that the process shows maximum adsorption efficiency. According to this isotherm, the concentration of ions adhering to the sorbent surface escalates as the adsorbent concentration rises, potentially allowing for the formation of multiple layers. When the adsorption intensity (n) surpasses one, it signifies the ease of isolating ions from the solution and, consequently, the feasibility of the adsorption process. The isothermal parameters calculated for the adsorption study of sunset yellow and tartrazine using synthesized FeNPs were tabulated in Table 1. The Langmuir and Freundlich isothermal graphs observed in the study were presented in Figure 9, respectively.

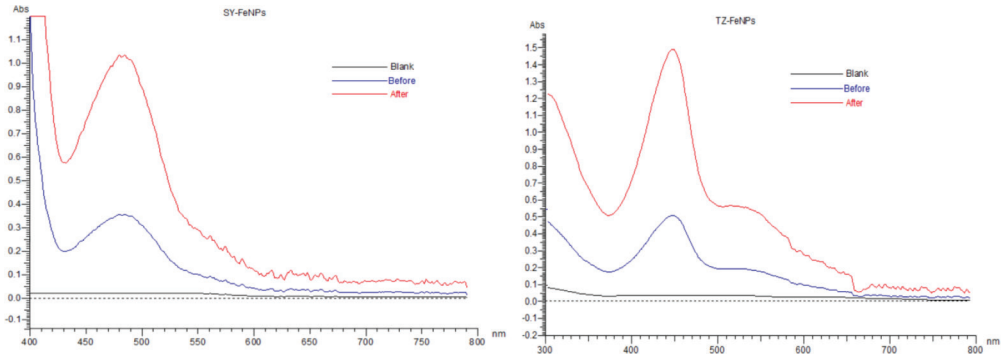


Figure 7. Overlay UV scanning spectra identified in the dye reduction study of synthesized nanoparticles.

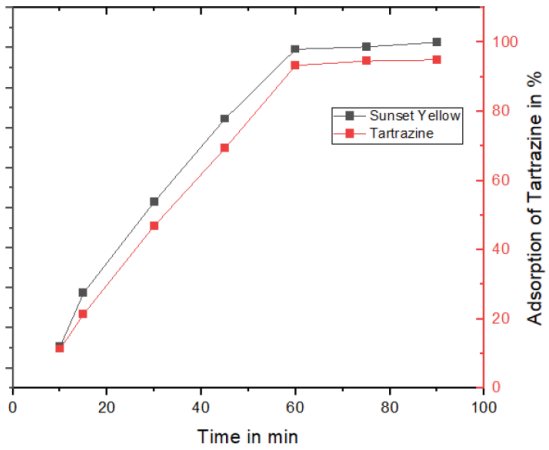


Figure 8. Adsorption study results of sunset yellow and tartrazine dyes using synthesized nanoparticles.

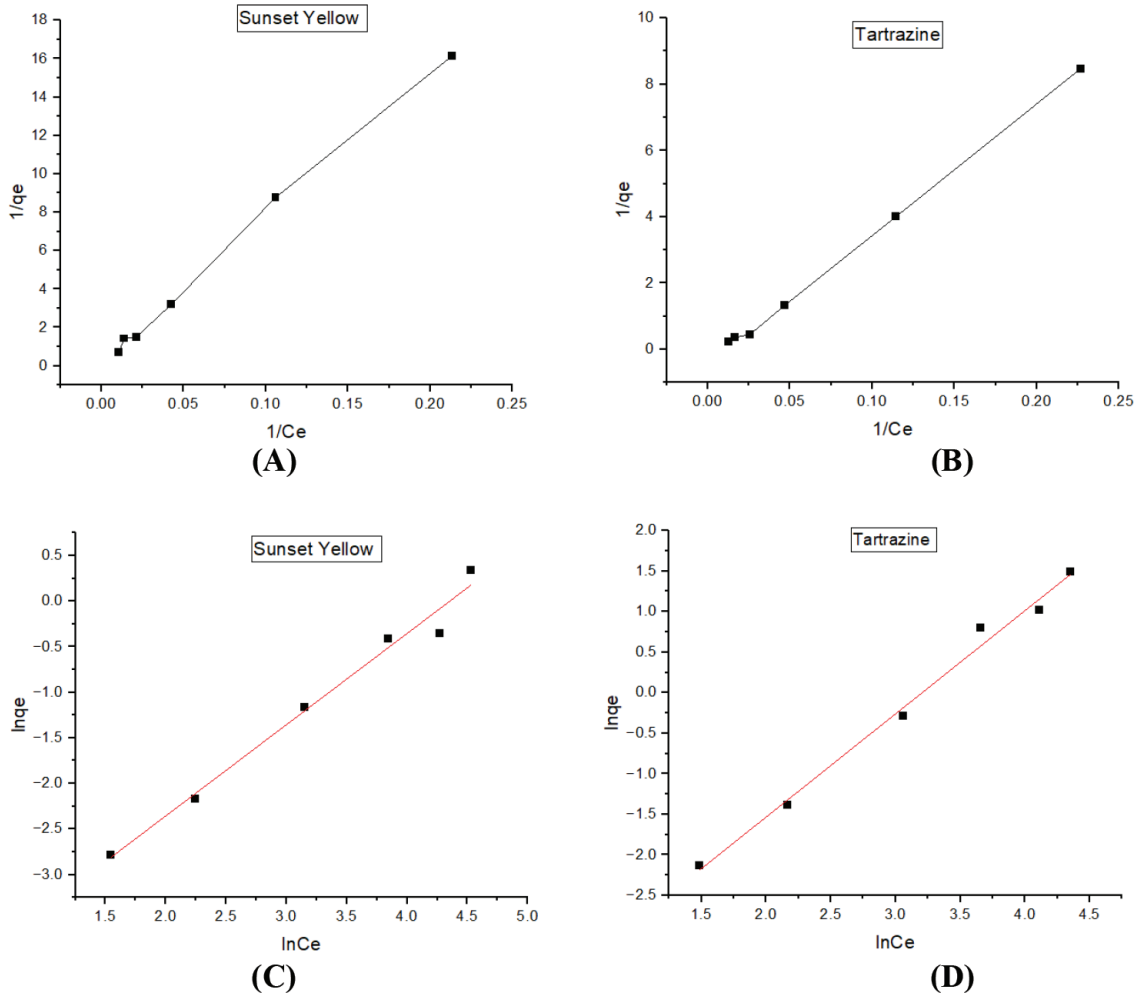


Figure 9. Adsorption isotherm model in the study. Langmuir isothermal graph for **(A)** sunset yellow and **(B)** tartrazine; Freundlich isothermal graph for **(C)** sunset yellow and **(D)** tartrazine.

3.3 Kinetics of Adsorption

The dye adsorption process using synthesized nanoparticles was evaluated using two different kinetic models, i.e., pseudo-first-order and pseudo-second-order models. The fitting results notably demonstrated a remarkable concurrence with the first-order model, as evidenced by the calculated correlation coefficient values. Furthermore, the application of the pseudo-first-order model yielded calculated adsorption capacities (qe) that closely matched the experimental values (Table 2), showcasing a perfect linear relationship across the entire range of dye concentrations. This exemplary fit to the first-order model suggests a kinetic mechanism in which both the dye ions and the adsorbent surface play essential roles, with the rate-determining step involving electron exchange between these two entities. The second order rate constant for the dye reduction study was noticed to be negative suggesting that the reaction doesn't follow second order and hence confirms that the adsorption follows pseudo-first order kinetics. The kinetic parameters were tabulated in Table 2 and pseudo-first-order kinetic plots were presented in Figure 10.

Table 1. Isotherm model parameters for the adsorption of sunset yellow and tartrazine using synthesized FeNPs

S. No	Equilibrium Model	Parameter	Results	
			Sunset Yellow	Tartrazine
1	Langmuir	q_{max} (mg/g)	76.29	47.22
		K_L (L/mg)	0.00134	0.00384
		R^2	0.998	0.99606
2	Freundlich	K_F (L/mg)	0.9994	0.9649
		R^2	0.992	0.9899

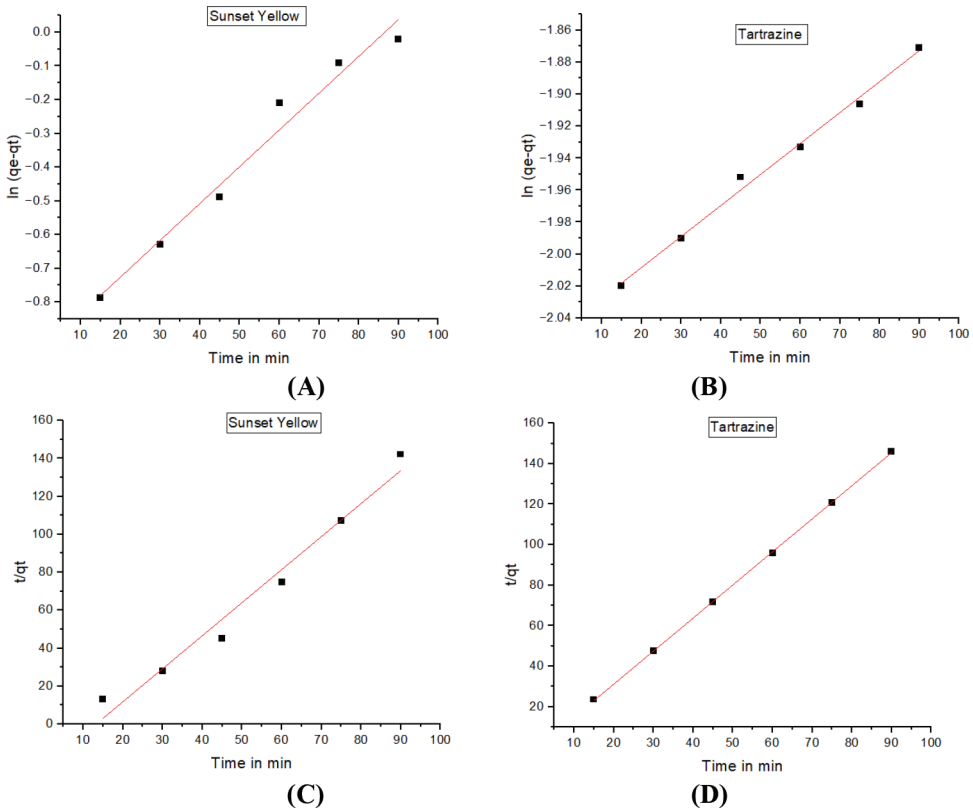


Figure 10. Kinetic plots observed during dye reduction study. Pseudo-first order plot observed for in the reduction of **(A)** sunset yellow and **(B)** tartrazine; Pseudo-first order plot observed for in the reduction of **(C)** sunset yellow and **(D)** tartrazine.

3.4 Stability and Recyclability of Nanoparticles

The chemical stability of FeNPs synthesized in this study was evaluated across a pH range from 2.0 to 10. In the stability analysis, the metal content of the nanoparticles was compared to those synthesized in our study, and the percentage of stability was calculated. The results achieved in the study illustrate that the synthesized nanoparticles maintained stability across the tested pH concentrations.

Assessing the reusability of the prepared nanoparticles was crucial for cost-effective analysis. In the initial cycle, the FeNPs displayed impressive reusability rates of 99.29 ± 0.229 and 98.79 ± 0.169 % for the adsorption of sunset yellow and tartrazine respectively. As the cycles progressed, there was a slight decline in reusability, with rates of 96.87 and 97.01 % for the adsorption of sunset yellow and tartrazine. This gradual decrease in efficiency may be attributed to the reduced availability of active sites within the nanoparticles due to the blockage of these sites by dye ions. In summary, the nanoparticles exhibited notable reusability with consistently high levels of adsorption efficiency.

The results achieved in this study were compared with various adsorbents reported in the literature and a summary of the study was tabulated in Table 3. The results confirm that the nanoparticles synthesized in the study were noticed to be an effective adsorbent for the removal of studied dyes.

Table 2. Dye adsorption kinetic models of synthesized nanoparticles

S. No	Kinetic Order	Parameter	FeNPs	
			Sunset Yellow	Tartrazine
1	First	K1	1.21×10^{-4}	2.15×10^{-5}
		qe (mg/g)	0.574	0.459
		R^2	0.987	0.987
2	Second	K2	-0.110	-0.107
		qe (mg/g)	0.574	0.459
		R^2	0.997	0.999

Table 3. Comparison of dye adsorption efficiency of nanoparticles synthesized in this study with the available literature.

S. No	Dye	Adsorbent	q_{max} (mg/g)	Reference
1	Sunset Yellow	*Cassava sievate* biomass derived nano carbon	22.40	[23]
2		Persulfate-based magnetic Fe_3O_4	46.7	[24]
3		Cadmium telluride nanoparticles loaded on activated carbon	19.94	[25]
4		Commercial Magnesium Oxide Nanoparticles	1.55	[26]
5		$NiFe_2O_4$ nanoparticles synthesised using the co-precipitation method	7.12	[27]
6		*Kigelia africana* leaf extract-mediated iron nanoparticles	76.29	This study
7	Tartrazine	Polypyrrole-coated tenorite nanoparticles	32.60	[28]
8		carbon nanotubes decorated with silver nanoparticles	27.18	[29]
9		*Cassava sievate* biomass derived nano carbon	30.06	[23]
10		Activated carbon doped with Copper oxide nanoparticles	19.81	[30]
11		$NiFe_2O_4$ nanoparticles synthesised using the co-precipitation method	6.33	[27]
12		*Kigelia africana* leaf extract-mediated iron nanoparticles	47.22	This study

4. Conclusion

This study presents the potential application of *Kigelia africana* (Lam.) Benth., biogenically synthesized iron nanoparticles as a highly effective nano-adsorbent for the decontamination of carcinogenic dyes such as sunset yellow and tartrazine. The study investigates the impact of various factors, including pH, contact time, temperature, and adsorbent dosage, on the removal of dyes and dyes, and these parameters are optimized for the process. Notably, the adsorption isotherms of iron nanoparticles for both dyes are found to be best described by the Langmuir model with maximum adsorption capacities. Hence, the nanoparticles synthesized in this study can exhibit outstanding adsorption and regenerative capabilities, making them a promising and suitable solution for the removal of toxic carcinogenic pollutants in water.

5. References

1. Lellis B, Fávaro-Polonio CZ, Pamphile JA, Polonio JC. Effects of textile dyes on health and the environment and bioremediation potential of living organisms. Biotechnol Res Innov. 2019; 3(2):275-90. https://doi.org/10.1016/j.biori.2019.09.001
2. Hossain MS, Das SC, Islam JM, Al Mamun MA, Khan MA. Reuse of textile mill ETP sludge in environmentally friendly bricks–effect of gamma radiation. Radiat Phys Chem. 2018; 151:77-83. https://doi.org/10.1016/j.radphyschem.2018.05.020
3. Wang DM, Environmental protection in clothing industry. Sustainable development. Proceedings of the 2015 International Conference on Sustainable Development; 2016. p. 729-735. https://doi.org/10.1142/9789814749916_0076
4. Orts F, Del Río AI, Molina J, Bonastre J, Cases F. Electrochemical treatment of real textile wastewater: Trichromy Procion HEXL®. J Electroanal Chem. 2018; 808:387-94 https://doi.org/10.1016/j.jelechem.2017.06.051
5. Hassan MM, Carr CM. A critical review on recent advancements of the removal of reactive dyes from dyehouse effluent by ion-exchange adsorbents. Chemosphere. 2018; 209:201-19. https://doi.org/10.1016/j.chemosphere.2018.06.043
6. Gomez M, Arancibia V, Rojas C, Nagles E. Adsorptive stripping voltammetric determination of tartrazine and sunset yellow in gelatins and soft drink powder in the presence of cetylpyridinium bromide. Int J Electrochem Sci. 2012; 7(8):7493-502. https://doi.org/10.1016/S1452-3981(23)15799-3
7. Alves SP, Brum DM, de Andrade ÉC, Netto AD. Determination of synthetic dyes in selected foodstuffs by high performance liquid chromatography with UV-DAD detection. Food Chem. 2008; 107(1):489-96. https://doi.org/10.1016/j.foodchem.2007.07.054
8. Dylan DF, Benjamin KS, Steve G, Morgan B, Jinsoo K, Aoife MF, David R. Decarbonizing the pulp and paper industry: A critical and systematic review of sociotechnical developments and policy options. Renew Sust Energ Rev. 2022; 167: 112706 https://doi.org/10.1016/j.rser.2022.112706
9. Yin H, Qiu P, Qian Y, Kong Z, Zheng X, Tang Z, Guo H. Textile wastewater treatment for water reuse: A case study. Processes. 2019; 7(1):34. https://doi.org/10.3390/pr7010034
10. Banat IM, Nigam P, Singh D, Marchant R. Microbial decolourization of textile-dyecontaining effluents: A review. Bioresour Technol. 1996; 58(3):217-27. https://doi.org/10.1016/S0960-8524(96)00113-7
11. Li XQ, Elliott DW, Zhang WX. Zero-valent iron nanoparticles for abatement of environmental pollutants: Materials and engineering aspects. Crit Rev Solid State Mater Sci. 2006; 31(4):111-22. https://doi.org/10.1080/10408430601057611
12. Huang L, Weng X, Chen Z, Megharaj M, Naidu R. Green synthesis of iron nanoparticles by various tea extracts: Comparative study of the reactivity. Spectrochim Acta A Mol. Biomol Spectrosc. 2014; 130:295-301. https://doi.org/10.1016/j.saa.2014.04.037
13. Batool F, Iqbal MS, Khan SU, Khan J, Ahmed B, Qadir MI. Biologically synthesized iron nanoparticles (FeNPs) from Phoenix dactylifera have anti-bacterial activities. Sci Rep. 2021; 11(1):22132. https://doi.org/10.1038/s41598-021-01374-4
14. Saranya S, Vijayarani K, Pavithra S. Green Synthesis of iron nanoparticles using aqueous extract of *Musa ornata* flower sheath against pathogenic bacteria. Indian J Pharm Sci. 2017; 79(5). https://doi.org/10.4172/pharmaceutical-sciences.1000280
15. Yakar A, Ünlü A, Yeşilçayır T, Bıyık İ. Kinetics and thermodynamics of textile dye removal by adsorption onto iron oxide nanoparticles. Nanotechnol Environ Eng. 2020; 5:1-2. https://doi.org/10.1007/s41204-020-0068-0
16. Singh J, Dutta T, Kim KH, Rawat M, Samddar P, Kumar P. Green synthesis of metals and their oxide nanoparticles: Applications for environmental remediation. J Nanobiotechnology. 2018; 16(1):1-24. https://doi.org/10.1186/s12951-018-0408-4
17. Da'na E, Taha A, Afkar E. Green synthesis of iron nanoparticles by *Acacia nilotica* pods extract and its catalytic, adsorption, and antibacterial activities. Appl Sci. 2018; 8(10):1922. https://www.mdpi.com/2076-3417/8/10/1922
18. Tyagi PK, Gupta S, Tyagi S, Kumar M, Pandiselvam R, Daştan SD, Sharifi-Rad J, Gola D, Arya A. Green synthesis of iron nanoparticles from spinach leaf and banana

peel aqueous extracts and evaluation of antibacterial potential. J Nanomater. 2021; 2021:1-1. https://doi.org/10.1155/2021/4871453

19. Alagiri M, Hamid SB. Green synthesis of α-2Fe_2O_3 nanoparticles for photocatalytic application. J Mater Sci Mater Electron. 2014; 25:3572-7. https://doi.org/10.1007/s10854-014-2058-0
20. Vadivel N, Yuvakkumar R, Suriyaprabha R, Rajendran V. Catalytic effect of iron nanoparticles on heterocyst, protein and chlorophyll content of Anabaena sp. Int J Green Nanotechnol. 2012; 4(3):326-38. https://doi.org/10.1080/19430892.2012.706185
21. Da'na E, Taha A, Afkar E. Green synthesis of iron nanoparticles by *Acacia nilotica* pods extract and its catalytic, adsorption, and antibacterial activities. App Sci. 2018; 8(10):1922. https://www.mdpi.com/2076-3417/8/10/1922
22. Ahmmad B, Leonard K, Islam MS, Kurawaki J, Muruganandham M, Ohkubo T, Kuroda Y. Green synthesis of mesoporous hematite (α-Fe_2O_3) nanoparticles and their photocatalytic activity. Adv Powder Technol. 2013; 24(1):160-7. http://dx.doi.org/10.1016/j.apt.2012.04.005
23. Chukwuemeka-Okorie HO, Ekuma FK, Akpomie KG, Nnaji JC, Okereafor AG. Adsorption of tartrazine and sunset yellow anionic dyes onto activated carbon derived from cassava sievate biomass. Appl Water Sci. 2021; 11:1-8. https://doi.org/10.1007/s13201-021-01357-w
24. Takdastan A, Pourfadakari S, Yousefi N, Orooji N. Removal of sunset yellow dye using heterogeneous catalytic degradation with magnetic Fe_3O_4/persulfate/ultrasound system. Desalin Water Treat. 2020; 197:402-12. https://doi.org/10.5004/dwt.2020.25956
25. Ghaedi M, Jah AH, Khodadoust S, Sahraei R, Daneshfar A, Mihandoost A, Purkait MK. Cadmium telluride nanoparticles loaded on activated carbon as adsorbent for removal of sunset yellow. Spectrochim. Acta A Mol Biomol Spectrosc. 2012; 90:22-7. https://doi.org/10.1016/j.saa.2011.12.064
26. Marzbani T, Khayatian G. Application of magnesium oxide nanoparticles for sunset yellow removal in aqueous solutions: Adsorption isotherm, kinetic, and thermodynamic studies. Iran J Chem Chem Eng. 2022. https://doi.org/10.30492/IJCCE.2022.529057.4696
27. Zandipak R, Sobhanardakani S. Synthesis of $NiFe_2O_4$ nanoparticles for removal of anionic dyes from aqueous solution. Desalin Water Treat. 2016; 57(24):11348-60. https://doi.org/10.1080/19443994.2015.1050701
28. Srivastava V, Maydannik P, Sharma YC, Sillanpää M. Synthesis and application of polypyrrole coated tenorite nanoparticles (PPy@ TN) for the removal of the anionic food dye 'tartrazine' and divalent metallic ions viz. Pb (II), Cd (II), Zn (II), Co (II), Mn (II) from synthetic wastewater. Rsc Advances. 2015; 5(98):80829-43. https://doi.org/10.1039/C5RA14108G
29. Goscianska J, Pietrzak R. Removal of tartrazine from aqueous solution by carbon nanotubes decorated with silver nanoparticles. Catal Today. 2015; 249:259-64. https://doi.org/10.1016/j.cattod.2014.11.017
30. Rad AJ. Synthesis of copper oxide nanoparticles on activated carbon for pollutant removal in Tartrazine structure. J Compos Compd. 2020; 2(3):99-104. https://doi.org/10.29252/jcc.2.2.6